Dynamical Instability of Holographic QCD at Finite Density

Wu-Yen Chuang[1], Shou-Huang Dai[2], Shoichi Kawamoto[2], Feng-Li Lin[2], Chen-Pin Yeh[3]

[1] *NHETC, Department of Physics, Rutgers University*
126 Frelinghuysen Rd, Piscataway, New Jersey 08854, USA
[2] *Department of Physics, National Taiwan Normal University, Taipei, Taiwan*
[3] *Department of Physics, National Taiwan University, Taipei, Taiwan*

Abstract

In this paper we study the dynamical instability of Sakai-Sugimoto's holographic QCD model at finite baryon density. In this model, the baryon density, represented by the smeared instanton on the worldvolume of the probe $D8$-$\overline{D8}$ mesonic brane, sources the worldvolume electric field, and through the Chern-Simons term it will induces the instability to form a chiral helical wave. This is similar to Deryagin-Grigoriev-Rubakov instability to form the chiral density wave for large N_c QCD at finite density. Our results show that this kind of instability occurs for sufficiently high baryon number densities. The phase diagram of holographic QCD will thus be changed from the one which is based only on thermodynamics. This holographic approach provides an effective way to study the phases of QCD at finite density, where the conventional perturbative QCD and lattice simulation fail.

1   Introduction

The quantum chromodynamics (QCD) at high baryon density has implications for physics in many fields, such as the possible existence of quark matters in the core of compact stars. However, unlike the physics for QCD at finite temperature, it is difficult to directly probe such a regime theoretically, even from the first principle numerical simulations. This is mainly due to the complex fermion determinant at finite density, which causes the sign problem in simulation.

Despite that, it was conjectured that there is a color superconducting ground state for QCD at high enough density[1], similar to the BCS mechanism for the formation of Cooper pairs of quarks near the Fermi surface. Since the Fermi momentum plays the role of an additional energy scale, we can apply the perturbative techniques in the regime of ultra-high density. However, at moderate density where the most interesting physics dwells, QCD is strongly coupled and it is hard to have reliable treatments.

Instead, one can consider QCD at large N_c (number of color) limit to probe the above non-perturbative regime of finite density. This can be done either by using the renormalization group improved perturbative technique for small ' t Hoof coupling, or by studying the holographic dual gravity for large 't Hooft coupling. For the former case, Deryagin, Grigoriev and Rubakov (DGR)[2] noticed that color superconductivity will be suppressed in the large N_c limit since the Cooper pair of quarks is not color singlet and its formation is diagramtically non-planar. Moreover, they found that there is a new dynamical instability for the formation of chiral density wave whose wave number is the twice of the Fermi momentum [2, 3], i.e., a spatially modulated phase. This can be understood as the standing wave from the formation of quark-hole pairs.

On the other hand, the study of the gravity duals of large N_c $\mathcal{N} = 4$ Super-Yang-Mills(SYM) or QCD are shown to be able to capture many essential features of real QCD at high temperature and finite density such as what happened at RHIC. Indeed, a pioneering work by Domokos and Harvey[4] has shown that the bulk Chern-Simons term will induce a dynamical instability to form the DGR-like modulated phase in the zero temperature holographic QCD from a bottom-up approach. Recently the interest in the dynamical instability induced by the Chern-Simons term is revived by Nakamura, Ooguri and Park in [5]. They have explicitly shown that the new modulated phase is the helical wave of a holographic $U(1)$ current. These motivate us to study the same issue in the top-down approach of the holographic QCD, i.e., Sakai-Sugimoto model[6, 7] at finite temperature[8] and finite density[13]. The advantage of the top-down approach enables us to understand how marginal the above dynamical instability is in a more consistent and systematical way. In our model we figure out a window for modulated phase of chiral helical wave at high temperature case as shown in Fig. 1.

In the next section, we will briefly review the holographic QCD proposed by Sakai and Sugimoto[6, 7], and then study thermodynamics of its generalization to the case with finite temperature and finite baryon density[13]. In Sakai-Sugimoto model the meson is dual to a pair of connected $D8$ and $\overline{D8}$ branes, and the baryon is dual to $D4$ branes wrapping on the internal S^4[9]. There is a pulling force on $D8$ exerted by the wrapped $D4$ whose strength is proportional to the baryon density. This

geometrizes the change of QCD vacuum by the presence of finite baryon density. In section 3 we discuss the dynamical instability in holographic QCD and derive the master equation for it, and in section 4 we discuss our numerical analysis to find out such an instability. The physical result of our analysis is summarized in the phase diagram as shown in Fig. 1. Finally, we conclude the paper in section 5.
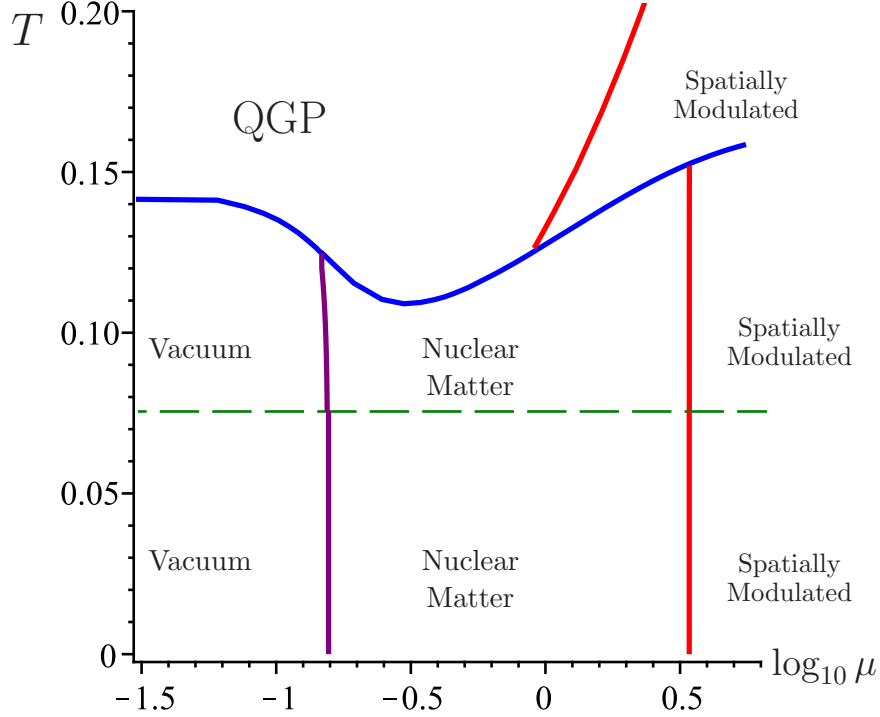

Figure 1: Phase diagram of our holographic QCD model at finite temperature and finite baryon density. The horizontal dashed line around $T = 0.075$ separates the low temperature (LT) and the high temperature (HT) phases. The left two purple lines, almost vertically straight in both of LT and HT phases, separate the nuclear matter phase and the vacuum phase where the baryon density vanishes. The horizontal curved blue line in the high temperature phase, starting from $T \simeq 0.14$, is the phase boundary between the nuclear matter or the vacuum phase, and the QGP phase. This line is determined thermodynamically. The three red lines on the right, inside the nuclear matter phase of both LT and HT phases and also in the QGP phase, denote the onset of dynamical instability in each phase. On the right of these lines, the system may be in a spatially modulated phase, though we do not discuss the stability of this modulated phase in the paper. The parameters (whose meaning will be clear in Section 2 and 4) are set to be $R = 1$, $L = 0.53$ and $\kappa \simeq 1.018$.

2 The Model of Holographic QCD

The Sakai-Sugimoto(SS) model consists of N_f pairs of $D8$ and $\overline{D8}$ branes embedded in the near horizon geometry of N_c $D4$ branes on a Scherk-Schwarz circle, which completely breaks the supersymmetry. The size of the circle basically controls the mass scale of the unwanted fields. The configuration can be summarized as follows:

$$
\begin{array}{ccccccccccc}
 & 0 & 1 & 2 & 3 & (4) & 5 & 6 & 7 & 8 & 9 \\
N_c\ D4 & \times & \times & \times & \times & \times & & & & & \\
N_f\ D8\overline{D8} & \times & \times & \times & \times & & \times & \times & \times & \times & \times
\end{array}
\tag{1}
$$

The x^4 direction is the Scherk-Schwarz circle with the anti-periodic boundary condition for fermionic fields.

The probe $D8$ branes have the embedding function $x_4 = x_4(U)$ and extend in the other 8 dimensions, where U is the radial coordinate of the background $D4$ brane geometry. The embedding function can be determined by solving the equations of motion of the $D8$ DBI action. In [6, 7] the authors found that there is a smooth interpolation of the $D8$-$\overline{D8}$ pair from the DBI action analysis, which was then interpreted as the chiral symmetry breaking of QCD. In this phase, the background geometry is described by (3), the dual effective QCD is confined[8] and the degrees of freedom are hadronic. By changing the time direction to a thermal circle, we can introduce temperature into the model. At a critical temperature, the geometry has a phase transition and becomes another geometry with horizon[8, 12]. This is the high temperature phase that corresponds to the deconfined phase of QCD and will be described in section 2.2 in detail.

In AdS_5/CFT_4 correspondence, the baryons are the $D5$ branes wrapping on the S^5. The RR-flux is coupled to the gauge field on the $D5$ worldvolume and becomes a source for the gauge field. In order to cancel the tadpole, there will be N_c strings attached to the $D5$ which looks like a pointlike particle in AdS_5[9]. Similar constructions of holographic baryons were done for SS model, which is carried out by wrapping $D4$ branes on the internal S^4[10, 11], and further smearing the $D4$ charges in the non-compact directions for the discussions of QCD phase diagram[13]. The $D4$ charge density then plays the role of baryon number density in the dual QCD. From the point of view of the probe $D8$, the wrapped $D4$'s are also regarded as instantons on the $D8$ worldvolume. However, it turns out that the complete treatment of the baryons as the world-volume instantons is quite difficult and is yet unknown. Thus we include the energy contribution of the instanton as $D4$-brane DBI action, which was done in [13]. Below we will review this results that will provide the background configuration for our further study of modulated phase instability.

After wrapping the $D4$, we also have to include the Chern-Simons(CS) action on the $D8$ brane

$$
S_{CS} = T_8 \int C_{p+1} \wedge \text{tr} \exp(2\pi\alpha' F)
\tag{2}
$$

if there is non-trivial RR potential C_{p+1} generated by Dp-brane or non-trivial gauge curvature F on the $D8$ worldvolume. We will regard the wrapped $D4$ branes as sources to generate non-trivial F along $1, 2, 3, U$ directions and focus on the coupling of $U(1)$ part to $SU(N_f)$ part of the gauge

field on $D8$ brane. The $SU(N_f)$ part of the gauge field is the anti-self dual connection whose second Chern character is the number of $D4$ branes, i.e., $\frac{1}{8\pi^2}\text{tr}\,F^2 = N_f n_4 \delta(U - U_c)d^3x dU$, where n_4 is the dimensionless instanton number density and we also take the total number of the instanton to be a multiple of N_f.

2.1   Thermodynamics of the low temperature phase

We first consider the low temperature (LT) phase of QCD in which the quarks and gluons are confined, and the chiral symmetry is spontaneously broken. The $D4$ background solution dual to the low temperature phase of QCD is given by [12],

$$ds^2 = \left(\frac{U}{R}\right)^{\frac{3}{2}}(\eta_{\mu\nu}dx^\mu dx^\nu + h(U)dx_4^2) + \left(\frac{R}{U}\right)^{\frac{3}{2}}\left(\frac{dU^2}{h(U)} + U^2 d\Omega_4^2\right)$$

$$F_4 = \frac{(2\pi)^3\ell_s^3 N_c}{\Omega_4}\epsilon_4, \quad e^\phi = g_s\left(\frac{U}{R}\right)^{\frac{3}{4}}, \quad h(U) = 1 - \frac{U_{KK}^3}{U^3}, \quad x_4 \sim x_4 + \frac{4\pi R^{3/2}}{3U_{KK}^{1/2}}, \tag{3}$$

where $\mu, \nu = 0, 1, 2, 3$, U is the radial direction, the $d\Omega_4^2$ and ϵ_4 are the metric and volume form of the S^4 of unit radius, and $R^3 = \pi g_s N_c \ell_s^3$. This geometry has a cigar shape terminated at $U = U_{KK}$.

The DBI action and CS action in terms of the $D8$ brane embedding function $x_4(U)$ and the electric field $E(U) := -A_0'$ are the following [1]

$$S_{DBI} = -N \int dU U^4 \sqrt{hx_4'^2 + (1/U)^3(1/h - A_0'^2)}\,, \tag{4}$$

$$S_{CS} = \frac{N_c}{8\pi^2}\int_{M_4 \times R_+} A_0 \text{tr}\,F^2 = N n_b \int dU \delta(U - U_c)A_0\,, \tag{5}$$

where the $'$ is the derivative with respect to U, $\beta := \int dx_0$ is the inverse temperature, $V_3 := \int dx_1 dx_2 dx_3$, Ω_4 is the volume of unit S^4, $N := \frac{T_8 R^5 N_f V_3 \beta \Omega_4}{g_s}$, and the dimensionless baryon number density is $n_b := \frac{N_c N_f n_4 V_3 \beta}{2\pi\alpha' R^2 N}$. Here, for the DBI action, we only include the $U(1)$ part of the gauge field and neglected the contribution from the $SU(N_f)$ part.[2] The contribution from the $SU(N_f)$ part is basically the energy of the instantons and this will be included as D4-brane action on S^4 when the stationary condition is considered. The D4-brane action on S^4 at $U = U_c$ is given by

$$S_{D4} = - N_4 T_4 \int d\Omega_4 d\tau e^{-\Phi}\sqrt{-\det g}\Big|_{U=U_c} = \frac{N n_b}{3}U_c\,, \tag{6}$$

where $N_4 = N_f n_4 V_3/R^3$ is the number of D4-branes.

One can derive the equations of motion from (4), and then solve for $x_4(U)$ and $E(U)$:

$$x_4' = \pm U^{-\frac{3}{2}}\frac{\sqrt{H_0 \sin^2\theta_c}}{h\sqrt{H - H_0 \sin^2\theta_c}}\,, \qquad E = -n_b U^{\frac{3}{2}}\frac{1}{\sqrt{H - H_0 \sin^2\theta_c}}\,, \tag{7}$$

---

[1]In the following we re-scale the coordinates (U, x_0, x_1, x_2, x_3) by factor of R so that they are dimensionless, and also rescale $U(1)$ part of the gauge fields by factor of $\frac{\sqrt{2N_f}R}{2\pi\alpha'}$. Also note that these actions describe the upper half of the connected D8-branes, and then the actual action is twice of this. To investigate the phase structure, it is sufficient to look at this half and we will consider only this part of the action.

[2]It is not difficult to see that the contributions from this non-Abelian part is completely mixed, in a complicated way, with the Abelian part functions we will now solve, and also the complete form of the contribution is yet unknown.
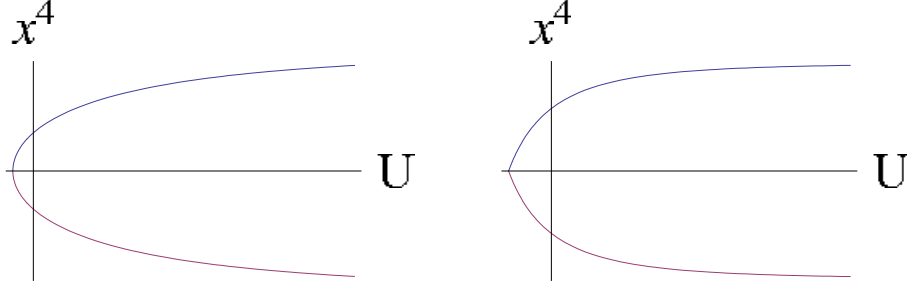
4

Figure 2: Smooth $D8 - \overline{D8}$ for $n_b = 0$ $D8 - \overline{D8}$ with a cusp for nonzero n_b

where

$$H(U) = U^3 h(U) \, (U^5 + n_b^2), \ H_0 = H(U_c), \ \tan \theta_c = \sqrt{g_{44}/g_{UU}} \ x_4'|_{U=U_c} \ , \tag{8}$$

where g_{44} and g_{UU} refer to the corresponding factors in the metric (3).

To further solve (7), we need to impose the fixed length condition, i.e.,

$$L = \int_{U_c}^{\infty} dU \, x_4', \tag{9}$$

where $2L$ is the UV separation of $D8$ and $\overline{D8}$ along x_4-direction. The $D8$-$\overline{D8}$ profiles for zero and non-zero n_b are shown in Fig. 2. Note that this parameter L is particular to the SS model and does not correspond to any physical parameter in the real QCD. We will set $L = 0.53$ and $U_{KK} = 0.1$ throughout our analysis. This choice is partly motivated by the physical parameter choice of SS model and will be explained more in Section 4.

Geometrically, the above solution arises from the balance between the $D8$'s tension from the DBI part and the pulling by $D4$ wrapping on S^4. As a result, the $D8$ profile develops a cusp at IR end $U = U_c$ with a cusp angle θ_c appearing as a constant of integration in (7) and (8). This is determined by the force balance solution

$$\left(\frac{1}{\sqrt{g_{UU}}} \frac{dH_{D8}}{dU_c} + \frac{1}{\sqrt{g_{UU}}} \frac{dS_{D4}^E}{dU_c} \right)_{\text{on-shell}} = 0 \ , \tag{10}$$

where $H_{D8} = -S_{DBI} + \int dU \Pi_{A_0} A_0'$, S_{D4}^E denotes the Euclidean D4 DBI action with Π_{A_0} the conjugate momentum of A_0, and the total derivative is defined as $\frac{d}{dU_c} := \frac{\partial}{\partial U_c} + \left(\frac{\partial x_4'(U)}{\partial U} \Big|_{\substack{U=U_c \\ n_b, L \ fixed}} \right) \cdot$ $\frac{\delta}{\delta x_4'(U)}$ which should be performed before imposing the on-shell condition. Solving (10)[3] for the cusp angle θ_c yields

$$\cos^2 \theta_c = \frac{h(U_c)}{9} \frac{n_b^2}{n_b^2 + U_c^5}. \tag{11}$$

Note that as n_b reduces to 0, $\theta_c = \pi/2$ and the cusp becomes a smooth tip.

For a given n_b, the cusp location U_c can be determined by solving the fixed length condition (9). This relation is displayed in Fig. 3(a). As n_b increases, D4-brane pulls the cusp towards the tip of the cigar-like space, but at some point the tension of D8-brane overcomes the pulling force and the position of the cusp goes to large U region.

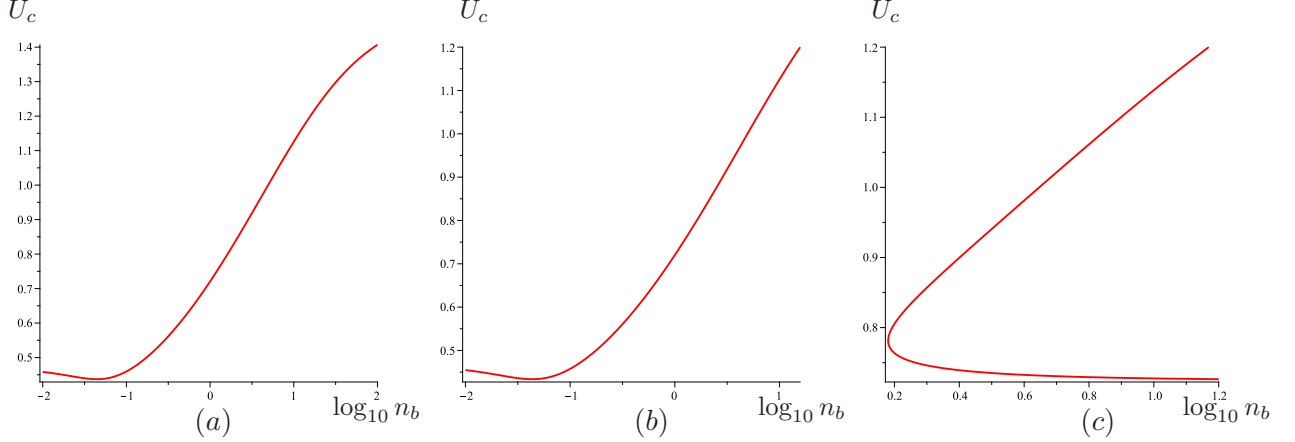[3]To solve it, one may need to use the trick pointed out in the footnote 6 of [14].

Figure 3: The cusp position U_c against $\log_{10} n_b$ at $U_{KK} = 0.1$, $L = 0.53$ for (a) the low temperature phase; and (b) and (c) are the high temperature phase at $T = 0.0755$ (or $U_T = 0.1$) and $T = 0.1997$ ($U_T = 0.7$), respectively. (See sec. 2.2).

Next, we discuss the thermodynamics of the $D8$-$\overline{D8}$ branes. We will neglect the back reaction from the probe branes so that the contribution to the free energy from the $D4$ background geometry will be the same for different configurations of probe branes, and can be omitted and considered separately. Therefore, the grand canonical potential of holographic QCD is given by [16]

$$\Omega_{D8}(T,\mu) = \frac{1}{N} \left(S_{DBI}^{E}\big|_{\text{on-shell}} + S_{CS}^{E}\big|_{\text{on-shell}} \right), \qquad (12)$$

where E denotes the Euclidean action, while the Helmholtz free energy is[4]

$$
\begin{aligned}
F_{D8}(T, n_b) &= \mu n_b + \Omega_{D8}(T,\mu) = \frac{1}{N} S_{DBI}^{E}\big|_{\text{on-shell}} + n_b \int_{U_c}^{\infty} A_0' \, dU \\
&= \int_{U_c}^{\infty} U^4 \sqrt{\left(h(U)(x_4')^2 + \frac{1}{U^3 h(U)} \right) \left(1 + \frac{n_b^2}{U^5} \right)} \, dU \Bigg|_{x_4' \,\text{on-shell}} ,
\end{aligned}
\qquad (13)
$$

where μ is the chemical potential defined by

$$\mu := A_0(U \to \infty). \qquad (14)$$

Note that the temperature dependence in the LT phase is trivial and the following expressions have actually no T dependence in this phase. The system contains also wrapped D4-branes, and its free energy is simply given by the Euclidean action (normalized by the factor N). Thus the total free energy is

$$F(T, n_b) = F_{D8}(T, n_b) + \frac{1}{N} S_{D4}^{E}. \qquad (15)$$

---

[4] In the second line of (13), A_0' had been replaced by x_4' by means of the equation of motion. Here we choose to express $F(T, n_b)$ by x_4' for the convenience of calculating the chemical potential μ. In the following, (16) is carried out as a chain-rule differentiation since F here is a on-shell quantity. Equivalently, one can also treat F as off-shell and use the functional variation method to derive μ. The result is the same.

From thermodynamics, the chemical potential is also obtained by

$$
\mu = \frac{\partial F}{\partial n_b}\bigg|_{T,L}
$$

$$
= \frac{\partial F_{D8}}{\partial n_b}\bigg|_{x'_4,U_c,T,L} + \frac{\partial F_{D8}}{\partial x'_4}\frac{\partial x'_4}{\partial n_b}\bigg|_{U_c,T,L} + \left(\frac{\partial F_{D8}}{\partial U_c} + \frac{1}{N}\frac{\partial S^E_{D4}}{\partial U_c}\right)\frac{\partial U_c}{\partial n_b}\bigg|_{x'_4,T,L} + \frac{1}{N}\frac{\partial S^E_{D4}}{\partial n_b}\bigg|_{x'_4,T,L}. \quad (16)
$$

Note that this formulation is under the implicit constraint of L being fixed. The second term on the right hand side vanishes, because $\frac{\partial F}{\partial x'_4}$ gives rise to an constant of motion inside the integral, and $\int_{U_c}^{\infty}\frac{\partial x'_4}{\partial n_b}\big|_{U_c} = \frac{dL}{dn_b} = 0$ since L is fixed[13]. The third term also vanishes due to the force balance condition (10) (note that $NF_{D8} = H_{D8}$). The remaining terms are consistent with the fixed length condition. As a result, the chemical potential reads [5]

$$
\mu = \int_{U_c}^{\infty} A'_0 dU + \frac{1}{N}\frac{\partial S^E_{D4}}{\partial n_b} = \int_{U_c}^{\infty} dU\, n_b \sqrt{\frac{U^3}{H(U) - H_c \sin^2\theta_c}} + \frac{U_c}{3}. \quad (17)
$$

The chemical potential μ as a function of n_b is displayed in Fig. 4(a). As n_b goes to zero, μ approaches a nonzero value. Below this value, there is no cusp configuration and then the system is described by the $D8$-$\overline{D8}$ configuration without instantons. This is called the vacuum phase[13]. In this phase, μ is a free parameter and we compare the grand canonical potential of the nuclear matter phase and the vacuum phase, and conclude that as long as the cusp configurations exist, the nuclear matter phase is always favored.
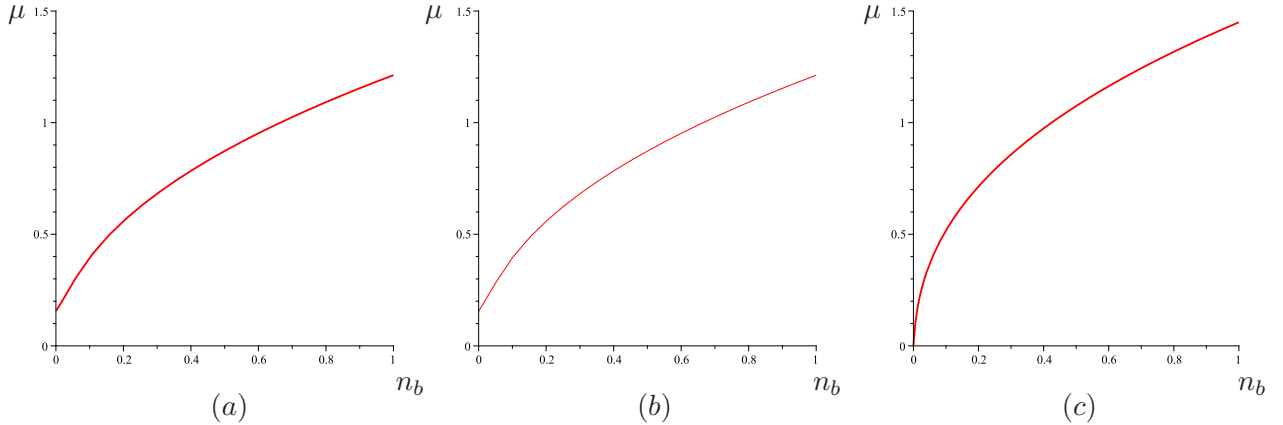

Figure 4: The chemical potentials versus n_b in: (a)the low temperature phase, (b) the high temperature nuclear matter phase at $T = 0.0755$(See sec. 2.2) and (c) the QGP phase at $T = 0.0755$(See sec. 2.2). In all the figures, the horizontal line denotes n_b and the vertical one μ.

---

[5]c.f. footnote 8 of [14].

2.2 Thermodynamics of the high temperature phase

Similarly, one can also consider the high temperature (HT) phase of holographic QCD, which is dual to the following metric[8]

$$ds^2 = \left(\frac{U}{R}\right)^{3/2}[-h(U)dt^2 + dx_1^2 + dx_2^2 + dx_3^2 + dx_4^2] + \left(\frac{R}{U}\right)^{3/2}\left[\frac{dU^2}{h(U)} + U^2 d\Omega_4^2\right],$$

$$h(U) = 1 - \frac{U_T^3}{U^3}. \tag{18}$$

The dilaton and the 4-form flux are the same as in (3). The Hawking temperature determined from the metric is $T := \frac{3}{4\pi}\sqrt{\frac{U_T}{R^3}}$ which is the temperature for holographic QCD.

The transition between the LT and the HT phases occurs at $T_c = \frac{3}{4\pi}\sqrt{\frac{U_{KK}}{R^3}} \simeq 0.0755$ [8]. Above T_c the temperature is varied by tuning U_T, and the dual QCD is deconfined. This critical temperature is obtained by comparing the free energies of the supergravity background of each phase. This is the background geometric transition which happens in the leading order at large N_c. Since the effect from the N_f quarks can be neglected in the planar limit, the boundary between the HT and LT phases is straight along the axis of μ, as shown by the dashed line in Fig. 1.

Embedding the $D8$ and $\overline{D8}$ branes in (18), by the same procedure in the LT case we can solve the $D8$-brane profile and the electric field, now together with the D4-brane action $S_{D4}^E = \frac{Nn_b}{3}\sqrt{h(U_c)}U_c$. The cusped solution is given by

$$x_4' = \pm U^{-3/2}\sqrt{\frac{H_0\sin^2\theta_c}{h(H - H_0\sin^2\theta_c)}} \;, \quad E = -n_b U^{3/2}\sqrt{\frac{h}{(H - H_0\sin^2\theta_c)}} \quad \text{(Nuclear matter)}. \tag{19}$$

The function H and the angle θ_c are also given by (8) and (11), with h taken from (18). Since the $D8$ and $\overline{D8}$ are joined at U_c with a cusp angle θ_c, with broken chiral symmetry this solution describes the nuclear matter in the dual QCD. Variation of U_c with n_b at $T = 0.0755$ (i.e., $U_T = 0.1$) and $T = 0.1997$ ($U_T = 0.7$) are displayed in Fig. 3(b) and (c). For lower temperature, the behavior is similar to that of the low temperature phase, and there always exists a solution. For higher temperatures, there will be no solution of the fixed length condition for small n_b, but these temperatures turn out to be in the QGP phase, which is described below, and then we will not face this missing solution problem.

The grand canonical potential, the Helmholtz free energy, and the chemical potential in the HT nuclear matter phase can be obtained formally from (12), the first line of (13) and (15), and (16) respectively. The chemical potential is given by $\mu = \int_{U_c}^\infty A_0' dU + \frac{1}{N}\frac{\partial S_{D4}^E}{\partial n_b} = \int_{U_c}^\infty dU\, n_b\sqrt{\frac{U^3 h(U)}{H(U) - H_0\sin^2\theta_c}} + \frac{U_c\sqrt{h(U_c)}}{3}$. The behavior μ against n_b is displayed in Fig. 4(b). Again, μ goes to a finite value as n_b vanishes, and there is also the vacuum phase in the high temperature region.

Moreover, unlike the LT case where the parallel $D8$-$\overline{D8}$ configuration is not allowed unless $L = 0$, in the HT phase we may have either the the chiral symmetry broken configuration (19), or the chiral symmetry restored one described by the parallel $D8$ and $\overline{D8}$:

$$x_4' = 0\;, \quad E = -A_0' = \frac{n_b}{\sqrt{U^5 + n_b^2}} \quad \text{(QGP)}. \tag{20}$$

Both branes extend in the radial direction from the horizon U_T to the boundary. Since the chiral symmetry is restored and the effective theory is deconfined, the configuration (20) describes the QGP phase. The chemical potential of the QGP phase is

$$\mu := \int_{U_T}^{\infty} A_0' dU = A_0(U \to \infty) , \qquad (21)$$

where $A_0(U_T)$ is set to 0 on the horizon to satisfy the regularity requirement. In the QGP phase there is of course no baryon degrees of freedom, so here we should regard the chemical potential as that of the liberated quarks and anti-quarks from the dissociation of baryons and mesons. Th chemical potential as a function of n_b is displayed in Fig. 4(c). For this QGP case, μ vanishes as n_b goes to zero.

To obtain the boundary between the nuclear matter and the QGP phase, we compare the grand canonical potential Ω, which are $\Omega_{\chi b}(T, \mu) = \int_{U_c}^{\infty} dU U^5 \sqrt{\frac{U^3 h(U)}{H(U) - H_0 \sin^2 \theta_c}}$ for the nuclear matter phase and $\Omega_{QGP}(T, \mu) = \int_{U_T}^{\infty} dU \frac{U^5}{\sqrt{U^5 + n_b^2}}$ for the QGP phase. Note that the each n_b in the above formulae takes different values in each phase, for the same T and μ. From our numerical calculation, we determine the phase boundary where the difference of the potential goes to zero. These are the boundary between the QGP and the nuclear matter in the high temperature phase in Figure 1. In this high temperature phase, there is also the vacuum phase where the D8-brane does not develop the cusp. The boundary between the vacuum and the nuclear matter phase is determined by $\lim_{n_b \to 0} \mu(n_b)$ for a given temperature, and by comparing the grand canonical potential the nuclear matter phase is again preferred if exists. The boundary between the QGP and the vacuum phase is also determined by comparing the grand canonical potential. The potential for the vacuum phase is given by $\Omega_{\text{vac}}(T) = \int_{U_c}^{\infty} dU \sqrt{\frac{U^{13} h(U)}{U^8 h(U) - U_c^8 h(U_c)}}$.

3   Dynamical Instability

To see if there is any dynamical instability of holographic QCD at finite baryon density, we need to consider the bulk fluctuations around the above background. We then solve the bulk fluctuations and derive the expectation values of the corresponding operators. If the expectation value grows with time, it suggests the vacuum is unstable and implies dynamical instability.

For our purpose, we turn on the fluctuations $y(x_\mu, U)$ for $D8$ profile and $f_{IJ}(x_\mu, U) := \partial_I a_J - \partial_J a_I$ for $D8$ gauge fields. Holographically, the fields a_i, a_U and y are dual to the chiral current $\langle J_{L,R}^i \rangle$, pion field $\langle \bar{q} \gamma^5 q \rangle$ and chiral symmetry violation $\langle \partial_\mu J_{L,R}^\mu \rangle$[18], respectively. If there are normalizable unstable (i.e., its magnitude grows with time) solutions for these bulk fluctuations, it implies the dynamical instability to new phases. For example, if exists, the modulated phase for a_i, as discussed in [5], is dual to helical structure of large N_c QCD; and the new modulated phases for a_U and y will be dual to the chiral density wave, a kind of DGR instability.

To obtain the field equations for the above bulk fluctuations, we expand the Lagrangian $L_{DBI} + L_{CS}$ up to quadratic order for both low and high temperature phases, and perform the corresponding

variations. The results are

$$\frac{U^5}{L_0}\left\{\frac{\Delta_p}{h}\partial_0^2 y - (1-\Delta_p E^2)\partial_i^2 y - \Delta_p x_4' E \partial_i f_{0i}\right\} - \left\{\frac{U^8 h}{L_0}\left(y' - \frac{x_4'}{L_0}L_1\right)\right\}' = 0 , \qquad (22)$$

$$\frac{U^5}{L_0}\left\{-\Delta_p x_4' E\,\partial_i^2 y + \left(\Delta_p(x_4')^2 + \frac{1}{U^3 h}\right)\partial_i f_{0i}\right\} + \left\{\frac{U^5}{L_0}\left(f_{0U} - \frac{E}{L_0}L_1\right)\right\}' = 0 , \qquad (23)$$

$$\frac{U^5}{L_0}\left\{\partial_0 f_{0U} - \frac{h}{\Delta_p}\partial_i f_{iU} - \frac{E}{L_0}\partial_0 L_1\right\} = 0 , \qquad (24)$$

$$\frac{U^5}{L_0}\left\{-\Delta_p x_4' E\,\partial_0\partial_i y + \left(\Delta_p(x_4')^2 + \frac{1}{U^3 h}\right)\partial_0 f_{0i}\right\} + \frac{L_0}{U^3}\partial_j f_{ij} + \left(\frac{U^5 h}{L_0\Delta_p}f_{iU}\right)'$$
$$-\kappa\epsilon_{ijk}(2A_0\partial_j f_{kU} - E f_{jk} + A_0\partial_U f_{jk}) = 0 , \qquad (25)$$

where L_0 and L_1 represent the expressions

$$L_0 = U^4\sqrt{h(x_4')^2 + U^{-3}\left(\frac{1}{\Delta_p} - E^2\right)} , \qquad L_1 = \frac{U^8}{L_0}\left(y'x_4'\,h - U^{-3}E\,f_{0U}\right). \qquad (26)$$

and the index p labels different phases for the factor Δ_p, such that $\Delta_{LT} := h$ and $\Delta_{HT} := 1$. Note that the formulation of h in the LT and HT cases should be correspondingly taken from (3) and (18) respectively.

Though these are coupled equations which cannot be decoupled in general, we can isolate the equation for $f_i := \frac{1}{2}\epsilon_{ijk}f_{jk}$ from the other bulk fluctuations by applying $\epsilon_{ijk}\partial_j$ to (25). We then arrive at the master equation

$$\left(\frac{U^5 h}{L_0\Delta_p}f_k'\right)' + \frac{L_0}{U^3}\left\{-\frac{\Delta_p}{h}\left(1 + \frac{E^2}{L_0^2}U^5\right)\partial_0^2 f_k + \partial_i^2 f_k\right\} + 2\kappa\epsilon_{ijk}E\partial_j f_i = 0 , \qquad (27)$$

in which $\Delta_p(x_4')^2 + \frac{1}{U^3 h} = \frac{\Delta_p}{h}\left(\frac{L_0^2}{U^8} + \frac{E^2}{U^3}\right)$ is used. Note that y, a_U and a_0 are decoupled. This is the similar equation discussed in [5] for the instability to form the modulated phase; however, the effective CS coupling is not a fixed constant as in [5] but given by

$$\kappa := \frac{n_b}{4\pi^2 n_4} = 288\pi^2\frac{1}{\lambda^2}\frac{U_{KK}}{R} , \qquad (28)$$

and thus it depends on the choice of the parameters like 't Hooft coupling $\lambda := g_{YM}^2 N_c$, but not on the instanton number density.

The parameter κ and the baryon number density n_b will turn out to govern the strength of instability to form the modulated phase as discussed in [5]. So when n_b and κ take a sufficiently large value, the dynamical instability would appear, as we will confirm by numerical calculation in the next section.

4 Numerical Results

In this section, we present our numerical analysis for possible dynamical instability, and the physical result is summarized in the phase diagram shown in Figure 1.

We start by summarizing our choice of the parameters. We set $M_{KK} = \frac{3}{2}\sqrt{\frac{U_{KK}}{R^3}}$ and 't Hooft coupling $\lambda = g_{YM}^2 N_c$ as $M_{KK} \simeq 950\text{MeV}$ and $\lambda \simeq 16.71$ (for example, [15]). This choice was set by using ρ-meson mass and the pion decay constant. We still have a freedom to choose the mass scale by R and then set $U_{KK}/R = 0.1$ and all the dimensions are adjusted by including R appropriately. This choice leads $\kappa \simeq 1.017980206$, and we choose the asymptotic half separation $L = 0.53$ [6].

We numerically solve the equations of motion derived in the previous section to find unstable modes. We use the standard "shooting" method to find the normalizable mode to determine the onset of the instability, which is given by the smallest available baryon number density that leads normalizable unstable modes at a given temperature.

First we consider the master equation (27). We assume the mode expansion $f_i = g_i(U)e^{-i(\omega t + k_j x^j)}$. Then, as explained in [5], the differential operator $\epsilon_{ijk}\partial_j$ has the eigenvalues $\pm k$ and 0 where $k = \sqrt{k^i k^i}$, and the equations of motion can therefore be diagonalized with respect to i independently of U. Note that the mode with zero eigenvalue turns out to be unphysical since it is in conflict with the Bianchi identity. Thus we diagonalize g_i and drop the subscript i for $g_i(U)$ from now on, and these three are distinguished by the eigenvalue that appears in the equation of motion (27).

We are looking for the normalizable solutions with negative ω^2. Near the boundary, the asymptotic solution is

$$g(U) \sim m + \frac{\nu}{U^{3/2}}, \tag{29}$$

where the leading constant m part gives the nonnormalizable mode and $\nu U^{-3/2}$ term is the normalizable mode, and m and ν are constants of integration. We are going to tune k for given parameters to find a solution that has vanishing m. Now the connected D8-brane configuration is symmetric under $x_4 \leftrightarrow -x_4$, and then two independent modes are either even or odd functions. This is equivalent to choose Neumann boundary condition $\{g(U_c) = 1, g'(U_c) = 0\}$ or Dirichlet one $\{g(U_c) = 0, g'(U_c) = 1\}$ at the connecting point[6]. Among these choices, we have observed that the first choice is prone to be unstable for various choices of the parameters. When we consider the other set of the equations of motion, we also take the same two boundary conditions for a_U fields, while for y and a_0 fluctuations we need to take the instantons into account. Since we have put the wrapped D4-branes at $U = U_c$ and have the boundary action (5), thus we take the boundary conditions that do not change this boundary term imposed as the background. So we take Dirichlet boundary condition for y so that the position of D4 brane would not change. Since the conjugate variable of a_0 with respect to U is a constant of motion, we put Neumann boundary condition for a_0, in order for this constant of motion, which is related to the instanton number density n_4, not

---

[6] Note that in this parameter choice, λ is not quite large and there exists a potential danger of having open string tachyons for too small L[6]. Our choice avoids this problem.
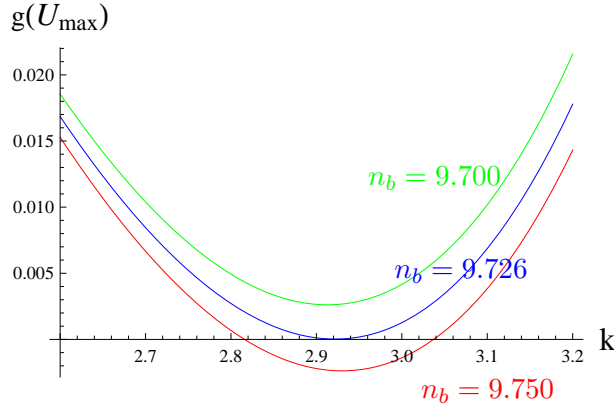
Figure 5: The numerical cartoon indicates the dynamical instability at $\omega = 0$ to form the modulated phase in low temperature phase by tuning n_b; namely, there exists a normalizable solution at critical n_b. The critical value of n_b is around 9.726.

to change. Finally, when we consider the instability for the QGP phase, we impose the in-falling boundary condition at the horizon, as usual.

We first analyze the marginal case $\omega^2 = 0$, where an unstable mode would start to appear. In the low temperature phase, we tune the baryon number density n_b to find the appearance of the instability. For the high temperature phase, we have another parameter U_T that gives the temperature T.

The unstable mode appearing at the smallest $n_b = n_{b(\text{crit})}$ can be considered to be the onset of the instability. The dynamical instability occurs for $n_b > n_{b(\text{crit})}$ at a given temperature T. Using this criterion, we determine the phase boundary between the "nuclear matter phase" and the "modulated phase" in the T–n_b plane. Note that we have not confirmed that this modulated phase stably exists, and we focus on drawing the phase boundaries. In Mathematica we implement a shooting method to look for the normalizable modes of $g(U)$ which vanish at large U. The Mathematica code is like the following schematically,

$$\texttt{NDSolve}[\{\texttt{EOM}(\texttt{k}, \omega^2 = 0) \texttt{ of } \texttt{g}, \texttt{g}[\texttt{U}_\texttt{c}] == 1, \texttt{g}'[\texttt{U}_\texttt{c}] == 0\}, \texttt{g}, \{\texttt{U}, \texttt{U}_\texttt{c}, \texttt{U}_\texttt{max}\}]. \tag{30}$$

Note that there are momentum dependences in the equation of motion. So we need to set up a do-loop to run over a range of momentum k and plot the diagram of k-$g[U_{max}]$, where U_{max} is chosen such that the sub-leading terms in $g(U_{max})$ can be dropped out and only the leading constant term m remains.

Here we provide the plot to show how we look for the dynamical instabilities in the low temperature phase; the plots in the HT phase at a given temperature are similar. Fig. 5 shows that the critical value of n_b at $\omega^2 = 0$ is around $n_b \approx 9.726$ since at this value there is a zero for $g(U_{max})$. That is to say we can find a normalizable solution at this critical value with $\omega^2 = 0$. Repeating this procedure for both low and high temperature phases, including QGP phase in the high temperature phase, the boundary to the the modulated phase (due to dynamical instability) is determined. Finally we translate these values of n_b into the chemical potential in the corresponding phase to the phase boundaries for μ–T diagram. The result is summarized in Fig. 1.

12

From our analysis, we see that n_b and κ govern the emergence of the instability, and for a given κ, which is determined by the choice of the parameters, we may choose a sufficiently large n_b to find the onset of the instability.
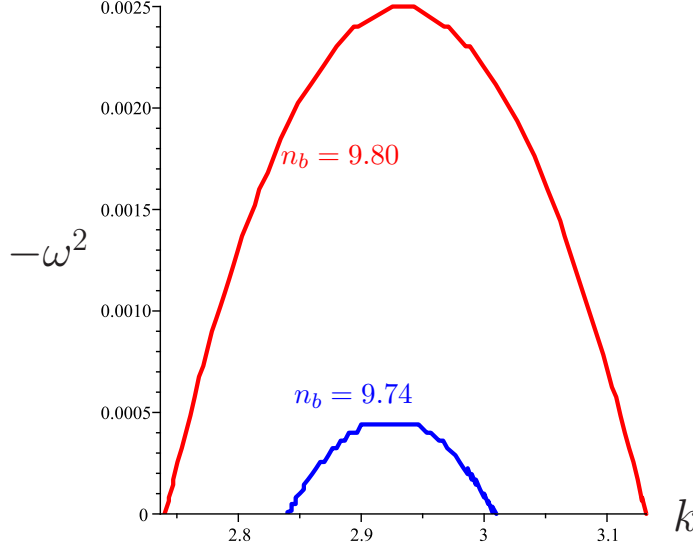

Figure 6: The dispersion of k and $-\omega^2$ for the normalizable unstable modes in the low temperature phase. The lower (blue) is for $n_b = 9.74$ and the higher (red) is for $n_b = 9.80$.

To confirm that the normalizable solutions we obtained indeed indicate instability, we next check the k dependence of $\omega(k)$. Fig. 6 is the plot of k dependence of $-\omega(k)^2$ at which the normalizable unstable solutions appear, for $n_b = 9.74$ and $n_b = 9.80$ in the low temperature phase. The horizontal axis is k and the vertical axis is $-\omega^2$. It shows that unstable modes appear between two marginal values of k for $n_b > 9.726$ as seen before.

Finally, we also analyze the instability of the other three modes. They cannot be decoupled, and we then take the common $\omega = 0$ and k for all and search for the normalizable mode for one of them. For the instability to appear, all of the fluctuations have to be normalizable[7]. For the QGP phase, there seems no normalizable mode. In the nuclear matter phases, we found a normalizable mode with $\omega = 0$ according to the combination of the boundary conditions, and it could be the onset of an instability. It appears at rather low baryon densities in general. However, the position of the onset depends very much on the choice of the boundary conditions, and we do not have the physical argument to fix this ambiguity at this moment. Therefore, we concentrate on the instability corresponding to f_i modes we discussed, and do not include into our phase diagram these might-be onsets of the instabilities from the other modes. It will then be nice if one could perform the full analysis and discuss the instabilities regarding other modes.

---

[7] Nonnormalizable modes may become normalizable as the frequency and the momentum change, however, we do not perform the full analysis here, but just the preliminary ones.

5 Conclusion

In this paper we study the dynamical instability of holographic QCD at finite density, which is usually difficult to attack by the conventional perturbative approach or the first principle lattice simulation due to the sign problem in the presence of finite chemical potential. One more advantage of holographic approach is to have the bulk geometric picture to illustrate the dynamical properties of QCD. For example, both the thermodynamical and dynamical instabilities are due to the pulling force of the $D4$ baryon branes exerted on the probe $D8$-$\overline{D8}$ meson branes. Our results are summarized in the phase diagram Fig. 1. The essential feature in Fig. 1 is the possible existence of the new modulated phase, which is missed by the homogeneity condition of thermodynamical consideration.

A key ingredient for the appearance of such a dynamical instability is that the baryon density induces the electric field in the holographic $D8$-$\overline{D8}$ brane, which couples to the QCD chiral current via the bulk Chern-Simons term. We find that the emergence of the instability is determined by the effective Chern-Simons coupling and the value of the baryon number density. By tuning the baryon number density high enough, a dynamical instability would appear, and this is consistent with the expectation from the previous large N_c analysis, at least for sufficient low temperatures. We have investigated the instabilities for several fluctuations on $D8$, and it should also be interesting to take the open string tachyon into account, which is dual to the chiral condensate and is an essential feature missed by the original Sakai-Sugimoto model, and to consider the dynamical instability with it.

Finally, we are left with an open question about the treatment of the non-Abelian contribution to the DBI action. As already stated, it is technically difficult to consistently include the effect, especially including the back-reaction to the D8-brane configuration. Therefore in the paper, we instead took only its energy into the system as the D4-brane action on the internal sphere. Though there has been a lot of literature on holographic QCD with finite baryon density, complete treatment of the non-Abelian instantons seems to be still an open problem. It is therefore very important to overcome this problem and to find a consistent way to include the whole contribution in the future.

Note added: During the preparation of the current version of the draft, we have been informed that Prof. Ooguri is also working on a similar problem about the instability in the QGP phase.

Acknowledgments

References

[1] M. G. Alford, K. Rajagopal and F. Wilczek, "QCD at finite baryon density: Nucleon droplets and color superconductivity," Phys. Lett. B **422**, 247 (1998) [arXiv:hep-ph/9711395].
M. G. Alford, K. Rajagopal and F. Wilczek, "Color-flavor locking and chiral symmetry breaking in high density QCD," Nucl. Phys. B **537**, 443 (1999) [arXiv:hep-ph/9804403].

[2] D. V. Deryagin, D. Y. Grigoriev and V. A. Rubakov, "Standing wave ground state in high density, zero temperature QCD at large N(c)," Int. J. Mod. Phys. A **7** (1992) 659.

[3] E. Shuster and D. T. Son, "On finite-density QCD at large N(c)," Nucl. Phys. B **573**, 434 (2000),

[4] S. K. Domokos and J. A. Harvey, "Baryon number-induced Chern-Simons couplings of vector and axial-vector mesons in holographic QCD," Phys. Rev. Lett. **99**, 141602 (2007), [arXiv:0704.1604 [hep-ph]].

[5] S. Nakamura, H. Ooguri and C. S. Park, "Gravity Dual of Spatially Modulated Phase," Phys. Rev. **D 81**, 044018 (2010), arXiv:0911.0679 [hep-th].

[6] T. Sakai and S. Sugimoto, "Low Energy Hadron Physics in Holographic QCD," Prog. Theor. Phys. **113** (2005) 843, [arXiv:hep-th/0412141].

[7] T. Sakai and S. Sugimoto, "More on a Holographic Dual of QCD," Prog. Theor. Phys. **114** (2005) 1083, [arXiv:hep-th/0507073].

[8] O. Aharony, J. Sonnenschein and S. Yankielowicz, "A holographic model of deconfinement and chiral symmetry restoration," Annals Phys. **322**, 1420 (2007), [arXiv:hep-th/0604161].

[9] E. Witten, "Baryons and Branes in Anti De Sitter Space," JHEP **9807** (1998) 006, [arXiv:hep-th/9805112].

[10] H. Hata, T. Sakai, S. Sugimoto and S. Yamato, "Baryons from instantons in holographic QCD," Prog. Theor. Phys. **117** (2007) 1157 [arXiv:hep-th/0701280].

[11] D. K. Hong, M. Rho, H. U. Yee and P. Yi, Phys. Rev. D **76**, 061901 (2007) [arXiv:hep-th/0701276]. D. K. Hong, M. Rho, H. U. Yee and P. Yi, JHEP **0709**, 063 (2007) [arXiv:0705.2632 [hep-th]].

[12] E. Witten, "Anti-de Sitter space, thermal phase transition, and confinement in gauge theories," Adv. Theor. Math. Phys. **2**, 505 (1998), [arXiv:hep-th/9803131].

[13] O. Bergman, G. Lifschytz and M. Lippert, "Holographic Nuclear Physics," JHEP **0711**, 056 (2007), [arXiv:0708.0326 [hep-th]].

[14] F. L. Lin and S. Y. Wu, "Holographic QCD with Topologically Charged Domain-Wall/Membranes," JHEP **0809**, 046 (2008), [arXiv:0805.2933 [hep-th]].

[15] K. Y. Kim, S. J. Sin and I. Zahed, "The Chiral Model of Sakai-Sugimoto at Finite Baryon Density," JHEP **0801** (2008) 002 [arXiv:0708.1469 [hep-th]].

[16] G. W. Gibbons and S. W. Hawking, "Action Integrals And Partition Functions In Quantum Gravity," Phys. Rev. D **15**, 2752 (1977).

[17] S. Kobayashi, D. Mateos, S. Matsuura, R. C. Myers and R. M. Thomson, "Holographic phase transitions at finite baryon density," JHEP **0702**, 016 (2007) [arXiv:hep-th/0611099].
S. Nakamura, Y. Seo, S. J. Sin and K. P. Yogendran, "Baryon-charge Chemical Potential in AdS/CFT," Prog. Theor. Phys. **120**, 51 (2008) [arXiv:0708.2818 [hep-th]].
D. Mateos, S. Matsuura, R. C. Myers and R. M. Thomson, "Holographic phase transitions at finite chemical potential," JHEP **0711**, 085 (2007) [arXiv:0709.1225 [hep-th]].

[18] E. Antonyan, J. A. Harvey, S. Jensen and D. Kutasov, "NJL and QCD from string theory," arXiv:hep-th/0604017.